PNAS RESEARCH ARTICLE | CELL BIOLOGY OPEN ACCESS

β-catenin turnover is regulated by Nek10-mediated tyrosine phosphorylation in A549 lung adenocarcinoma cells

Previn Dutt[a], Nasir Haider[b], Samar Mouaaz[a], Lauren Podmore[b], and Vuk Stambolic[a,b,1]

Edited by Nahum Sonenberg, McGill University, Montreal, Canada; received January 13, 2023; accepted March 8, 2024

β-catenin has influential roles affecting embryonic development, tissue homeostasis, and human diseases including cancer. Cellular β-catenin levels are exquisitely controlled by a variety of regulatory mechanisms. In the course of exploring the functions of the Nek10 tyrosine kinase, we observed that deletion of Nek10 in lung adenocarcinoma cells resulted in dramatic stabilization of β-catenin, suggestive of a Nek10 role in the control of β-catenin turnover. Nek10-deficient cells exhibited diminished ability to form tumorspheres in suspension, grow in soft agar, and colonize mouse lung tissue following tail vein injection. Mechanistically, Nek10 associates with the Axin complex, responsible for β-catenin degradation, where it phosphorylates β-catenin at Tyr30, located within the regulatory region governing β-catenin turnover. In the absence of Nek10 phosphorylation, GSK3-mediated phosphorylation of β-catenin, a prerequisite for its turnover, is impaired. This represents a divergent function within the Nek family, whose other members are serine-threonine kinases involved in different elements of the centrosomal cycle, primary cilia function, and DNA damage responses.

β-catenin | Nek10 | phosphorylation | lung cancer | metastasis

Significance

β-catenin is a bifunctional protein influencing both cell fate decisions and cell adhesion properties. Consequently, β-catenin deregulation significantly impacts a variety of cancers. A dramatic upregulation in β-catenin levels was observed following the deletion of the Nek10 tyrosine kinase in lung adenocarcinoma cells. Here, we identify a Nek10 target site on β-catenin, describe how Nek10 loss impaired β-catenin turnover, and assess the impact on tumorigenic potential including known β-catenin-controlled properties such as stem cell maintenance and metastatic propensity. Combined with the previously established Nek10 involvement in p53-mediated DNA damage responses, Nek10 can be regarded as a potential biomarker of lung adenocarcinoma and object for therapeutic targeting.

The Wnt/β-catenin signaling pathway is an evolutionarily conserved mechanism for control of cell fate throughout organismal lifespan, from embryonic development through adult tissue homeostasis. β-catenin has additional functions in cell adhesion, through its association with cadherins and other components of adherens junctions. Deregulation of the Wnt/β-catenin pathway impacts human diseases and is common in a variety of cancers (1). The archetypal β-catenin-driven oncogenic program is found in colorectal cancers, approximately 70% of which feature loss of function of the Adenomatous polyposis coli (APC) gene, leading to elevated β-catenin levels. Roughly 50% of hepatocellular carcinomas harbor various activating mutations targeting the Wnt pathway, with half of these found in the β-catenin gene (2). While upregulation of β-catenin does not by itself induce lung cancer, it has been shown to dramatically affect the progression of tumors driven by other oncogenic programs, such as Kirsten rat sarcoma viral oncogene homologue (KRAS) and Epidermal growth factor receptor (EGFR) activation (3, 4).

Wnt morphogens guide cell fate determination in target cells by promoting the appropriate spatiotemporal transcriptional programs (5). Fine-tuning of Wnt-mediated signaling is achieved through the concerted action of additional secreted factors, such as BMPs (bone morphogenetic proteins), as well as intracellular modifiers, acting either through the β-catenin pathway itself, or distinct developmental pathways capable of communicating with β-catenin throughput. More recently, the role of Wnt-β-catenin in regulating the stem cell niche in adult tissues, particularly the intestine, bone, and skin, has become better understood (6). For instance, a Wnt signaling gradient has been observed within intestinal crypts whereby Wnt ligands produced from underlying myoepithelial cells govern higher expression of Wnt target genes at the base of the crypt.

β-catenin levels are exquisitely controlled in cells. While the majority (~90%) of β-catenin is relatively stable and associated with cadherins in adherens junctions at the cell membrane, the remaining β-catenin is found in a highly dynamic signaling pool that is rapidly turned over in the absence of Wnt pathway signaling input (7). This turnover involves the recruitment of free cytoplasmic β-catenin into the Axin complex, followed by its sequential phosphorylation by Casein kinase 1 (CK1) at Ser45, and then by Glycogen synthase kinase-3 (GSK3) at Ser33, Ser37, and Thr41 (8, 9). These phosphorylation events promote recruitment of the β-Trcp ubiquitin E3 ligase, resulting in the ubiquitination and proteosomal degradation of β-catenin (10). APC is an indispensable component of the turnover complex, though its precise function and, more broadly, the mechanistic steps by which phosphorylated β-catenin is ubiquitinated and degraded remain unclear. Upstream signaling triggered by the binding of Wnt ligands to Frizzled receptors disrupts degradation of β-catenin, leading to its accumulation in the nucleus where it interacts

Author affiliations: [a]Princess Margaret Cancer Centre, University Health Network, Princess Margaret Cancer Research Tower, Toronto, ON M5G 1L7, Canada; and [b]Department of Medical Biophysics, University of Toronto, Princess Margaret Cancer Research Tower, Toronto, ON M5G 1L7, Canada

Author contributions: P.D. and V.S. designed research; P.D., N.H., and S.M. performed research; P.D., L.P., and V.S. analyzed data; and P.D. and V.S. wrote the paper.

The authors declare no competing interest.

This article is a PNAS Direct Submission.

[1]To whom correspondence may be addressed. Email: vuk.stambolic@uhn.ca.

This article contains supporting information online at https://www.pnas.org/lookup/suppl/doi:10.1073/pnas.2300606121/-/DCSupplemental.

Published April 29, 2024.

with the T-cell factor/lymphoid enhancer factor (TCF/LEF) transcriptional cofactors to activate target genes (11).

Nek10 is one of eleven members of the family of human Nek kinases implicated in regulation of various aspects of centrosome biology, primary cilia function, and DNA damage responses. While Nek2 and Nek5 are primarily involved in centrosome disjunction, a signaling module consisting of Nek6, Nek7, and Nek9 impacts several different mitotic functions, including centrosome positioning, spindle assembly, and cytokinesis (12). Beyond mitotic roles, Nek1 and Nek8, in particular, have been linked to ciliopathies such as polycystic kidney disease (13, 14).

Whereas the other members of the Nek family are serine-threonine kinases, Oriented Peptide Library Screening revealed that Nek10 has a preference for phosphorylation of tyrosine residues harboring phenylalanine, tryptophan, histidine, or leucine at the +1 position (15). Nek10 has been reported to interact directly with the Mitogen-activated protein kinase (MAP kinase) signaling module and promote phosphorylation of Extracellular signal-regulated kinase (ERK1/2) (16). While Nek10 is dispensable for ERK activation in response to mitogenic factors, it augments MAP kinase throughput related to a G2/M checkpoint engagement following UV irradiation. Most recently, it has been demonstrated that Nek10 also affects the p53-mediated response to DNA damage by phosphorylating p53 on Tyr327 (17).

Here, we report that Nek10 deficiency in A549 lung cancer cells results in an increase in β-catenin levels, both in the signaling and adherens junction pools. Elevation of β-catenin is a consequence of a reduction in Nek10-mediated phosphorylation at Tyr30 within the N-terminal regulatory region of the protein that governs its turnover. Reduced β-catenin Tyr30 phosphorylation, in turn, impaired GSK3-mediated phosphorylation events that are a prerequisite for subsequent recruitment of the β-Trcp E3 ubiquitin ligase and β-catenin turnover. At a cellular level, stabilization of β-catenin diminished the ability of A549 cells to form tumorspheres in suspension, grow in soft agar, and colonize mouse lung tissue following tail vein injections.

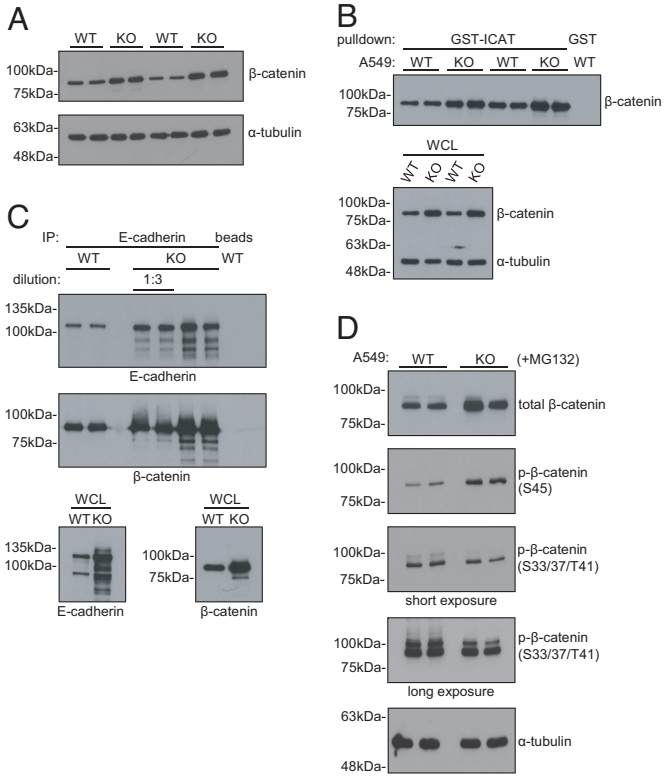

Fig. 1. Nek10 deletion in the A549 lung cancer line results in elevated β-catenin in both the signaling and adherens junction pools. (*A*) Total β-catenin levels in whole cell lysates of *NEK10*$^{+/+}$ and *NEK10*$^{\Delta/\Delta}$ A549 lines. α-tubulin was used as a loading control. (*B*) Total β-catenin pulled down by GST-ICAT from *NEK10*$^{+/+}$ and *NEK10*$^{\Delta/\Delta}$ A549 lysates. (*C*) The levels of β-catenin coimmunoprecipitating with E-cadherin in *NEK10*$^{+/+}$ and *NEK10*$^{\Delta/\Delta}$ A549 cells. (*D*) β-catenin phosphorylation at Ser45 and Ser33/Ser37/Thr41, relative to total β-catenin levels, in *NEK10*$^{+/+}$ and *NEK10*$^{\Delta/\Delta}$ A549 cells. Cells were treated with MG132. α-tubulin was used as a loading control.

Results

Nek10 Deletion in the A549 Lung Cancer Line Leads to Elevated Cellular Levels of β-catenin. The Nek10 kinase is highly expressed in both mouse and human lung tissue (*SI Appendix*, Fig. S1). Lower Nek10 expression correlates with better clinical outcomes in patients diagnosed with lung adenocarcinomas (*SI Appendix*, Fig. S2). To evaluate potential Nek10 functions in lung cancer biology, we deleted a Nek10 kinase domain exon encoding the critical DFG motif in A549 cells, as described previously (17). Initial characterization of various signaling pathways within the resulting knockout cell lines indicated a near fivefold increase in β-catenin protein abundance in multiple clonal lines (Fig. 1*A* and *SI Appendix*, Fig. S3*A*). Cell fractionation revealed that β-catenin was elevated in both the nuclear and cytosolic fractions of *NEK10*$^{\Delta/\Delta}$ A549 cells (*SI Appendix*, Fig. S3*B*). GST-ICAT (Inhibitor of β-catenin and TCF-4), a reagent designed to specifically capture the signaling pool of β-catenin (18), pulled down more β-catenin from Nek10-null than wild-type (WT) cell lysates (Fig. 1*B*). Moreover, elevated β-catenin reporter activity was observed in Nek10-deficient cells in the TOP-flash assay (*SI Appendix*, Fig. S3*C*). In *NEK10*$^{\Delta/\Delta}$ cells, more β-catenin also coimmunoprecipitated with E-cadherin than in their WT counterparts (Fig. 1*C*), consistent with an increase in β-catenin immunostaining observed at the cell membranes, where roughly 90% of β-catenin is typically localized within adherens junctions (*SI Appendix*, Fig. S3*D*). Elevated β-catenin in *NEK10*$^{\Delta/\Delta}$ cells was not a consequence of hyperactivation of the Wnt pathway, as phosphorylation of the Lrp6 coreceptor under both basal and Wnt-3a-induced conditions was indistinguishable in Nek10-proficient and -deficient cell lines (*SI Appendix*, Fig. S4*A*). Increased levels of β-catenin were also not a result of E-cadherin-mediated stabilization, as varying degrees of E-cadherin downregulation had no effect on β-catenin (*SI Appendix*, Fig. S4*B*).

The turnover of free β-catenin in cycling cells is highly dynamic, through proteasome-mediated degradation of hyperphosphorylated β-catenin protein species (Fig. 2*A*). When WT and *NEK10*$^{\Delta/\Delta}$ A549 cells were treated with MG132, to arrest proteosomal turnover, *NEK10*$^{\Delta/\Delta}$ cells displayed increased CK1-phosphorylated β-catenin compared to their WT counterparts, consistent with the elevated total β-catenin levels (Fig. 1*D*). In contrast, GSK3β-phosphorylated β-catenin levels were reduced in *NEK10*$^{\Delta/\Delta}$ cells (Fig. 1*D*). This was not the result of an overall change in the GSK3 activity, as determined by comparing the levels of GSK3 phosphorylation of one of its targets, Tau, in *NEK10*$^{+/+}$ *and NEK10*$^{\Delta/\Delta}$ cells (*SI Appendix*, Fig. S5).

Nek10 Phosphorylates β-catenin at Tyrosine 30. β-catenin turnover within the Axin destruction complex involves its phosphorylation by CK1 at Ser45, which primes for further GSK3β phosphorylation at Ser33, Ser37, and Thr41 (Fig. 2*A*) (10, 11). These sequential modifications, in turn, promote ubiquitination and proteosomal degradation of β-catenin. Although by sequence homology a member of the Nek family of serine-threonine

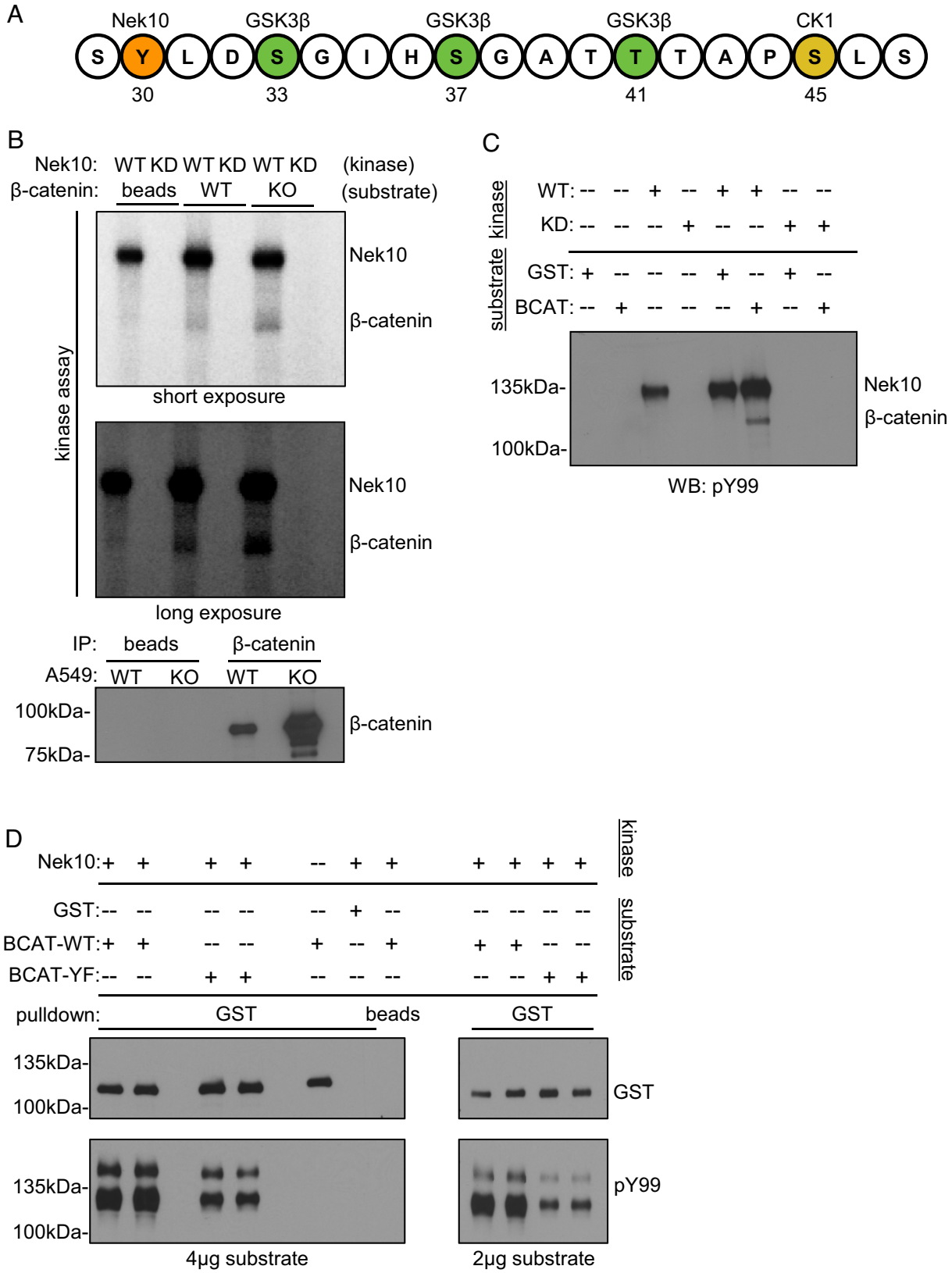

Fig. 2. Nek10 phosphorylates β-catenin at tyrosine 30. (*A*) Schematic of the locations of the critical N-terminal CK1 and GSK3 phosphorylation sites controlling β-catenin turnover, in relation to a putative Nek10-targeted site. (*B*) A radioactive kinase assay performed using recombinant WT or kinase-dead (KD) Nek10 to phosphorylate β-catenin from *NEK10*$^{+/+}$ and *NEK10*$^{\Delta/\Delta}$ A549 cells. (*C*) A nonradioactive kinase assay testing the ability of recombinant WT or KD Nek10 to tyrosine phosphorylate recombinant GST or GST-β-catenin (BCAT). (*D*) A nonradioactive kinase assay comparing the ability of recombinant WT Nek10 to tyrosine phosphorylate recombinant GST, as well as WT (BCAT-WT) or mutant (BCAT-Y30F) GST-β-catenin. In the mutant β-catenin, the putative Nek10 tyrosine target was changed to a nonphosphorylatable phenylalanine. The assay was carried out with either 4 μg (*Left*) or 2 μg (*Right*) of substrate.

kinases, Nek10 preferentially phosphorylates tyrosines, with phenylalanine, tryptophan, leucine, or histidine at the Tyr+1 position (15). β-catenin sequence contains a Tyr-Leu motif at Tyr30 which is proximal to the aforementioned CK1- and GSK3β-phosphorylation sites, as well as the subsequent ubiquitination sites at Lys19 and Lys49 (Fig. 2*A*).

In an in vitro ^{32}P kinase assay, Nek10 phosphorylated β-catenin immunopurified from both *NEK10*$^{+/+}$ and *NEK10*$^{\Delta/\Delta}$ A549 cells, with the level of phosphorylation corresponding to the relative amounts of β-catenin in the immunoprecipitates (Fig. 2*B*). Nek10 phosphorylated tyrosines in β-catenin, judged by using recombinant GST-β-catenin as substrate and pY99 anti-tyrosine antibody immunoblotting as readout (Fig. 2*C*). Nek10 phosphorylation of GST-β-catenin was dramatically reduced by the Y30F mutation, suggesting that Tyr30 is a Nek10 phosphorylation target in β-catenin (Fig. 2*D*).

Loss of β-catenin Tyrosine 30 Phosphorylation by Nek10 Impedes its GSK3-Mediated Phosphorylation, Leading to a Rise of Intracellular β-catenin Levels. To assess the effect of the β-catenin Tyr30 phosphorylation in cells, we expressed N-terminal HA-tagged WT and Y30F mutant β-catenin in HEK293T cells. Y30F β-catenin protein presented at considerably higher levels compared to the WT, suggestive of increased stability of the mutant (Fig. 3*A*). The exogeneous HA-β-catenin appropriately localized to both the (ICAT-associated) signaling and (E-cadherin-associated) adherens junction pools, with the mutant protein elevated in both (*SI Appendix*, Fig. S6 *A* and *B*). A similar effect was noted with C-terminal Myc-tagged β-catenin bearing the Y30F mutation (*SI Appendix*, Fig. S6*C*). Moreover, when the tagged β-catenin proteins were immunoprecipitated, the Y30F mutant exhibited less relative phosphorylation at GSK3β-target sites compared to the WT protein (Fig. 3*B*), similar to the effect observed in Nek10-null A549 cells (Fig. 1*D*).

To determine how differential phosphorylation impacted β-catenin turnover, we assessed association of β-catenin with its cognate E3 Ubiquitin ligase, β-Trcp, and found that the Y30F mutant displayed reduced β-Trcp engagement (Fig. 3*C*). Interestingly, a greater association of total and GSK3β-phosphorylated β-catenin with Axin was observed in HEK293T cells expressing exogeneous Y30F β-catenin, roughly correlating with the greater levels of β-catenin available for recruitment into the Axin complex (Fig. 3*D*). Collectively, these data suggest that Nek10 phosphorylates β-catenin at Tyr30 which promotes GSK3-mediated phosphorylation of β-catenin (Fig. 3*E*). In the absence of Nek10 phosphorylation, GSK3 phosphorylation, and all subsequent steps in the Axin-mediated turnover of β-catenin are impaired (Fig. 3*E*).

Levels of HA-tagged β-catenin and its Y30F mutant were assessed following treatment with either Wnt-3a, LiCl, or MG132, all of which impede its degradation at different points in the cascade (10, 19). To focus the analysis to the β-catenin signaling pool, apart from the more stable adherens junction pool, levels of HA-tagged β-catenin coimmunoprecipitating with Flag-ICAT were determined. Treatment of HEK293T cells with Wnt-3a resulted in stabilization of both WT and Y30F HA-tagged β-catenin (*SI Appendix*, Fig. S7*A*), demonstrating that the mutant protein retained responsiveness to upstream signaling. While the mechanisms by which Wnt stabilizes β-catenin are still not fully understood, the Y30F mutation contributed additional stabilization beyond that achieved by Wnt alone. A similar effect was observed when cells were treated with LiCl, a GSK3 inhibitor, or the proteosomal inhibitor, MG132, both of which led to elevated WT and Y30F β-catenin, with the Y30F mutant protein accumulating at higher levels (*SI Appendix*, Fig. S7 *B* and *C*).

WT, But Not Kinase-Dead (KD), Nek10 Reduces β-catenin Association with the Axin Complex. Immunoprecipitation experiments revealed a detectable, if weak, interaction between Nek10 and Axin, but not β-catenin (*SI Appendix*, Fig. S8 *A* and *B*). Intriguingly, overexpression of WT Nek10 caused a considerable reduction in the amount of Axin-associated β-catenin (*SI Appendix*, Fig. S8*C*), consistent with the increased Y30F β-catenin found in Axin immunoprecipitates (Fig. 3*D*). Expression of the KD Nek10 mutant failed to produce such an effect, further implying that the Nek10 input into β-catenin turnover is mediated by phosphorylation, rather than another mechanism.

Effect of Nek10 Loss on A549 Cell Function. To examine the potential physiological effects of Nek10 deficiency, we evaluated *NEK10*$^{+/+}$ and *NEK10*$^{\Delta/\Delta}$ A549 cell function in a series of in vitro and in vivo assays. In suspension tumorsphere-forming assays, a measure of stemness in cultured cells, A549 *NEK10*$^{\Delta/\Delta}$ cells were impaired compared to their WT controls (Fig. 4*A*). In soft agar growth assays, a measure of tumorigenicity in vitro, *NEK10*$^{\Delta/\Delta}$ A549 cells displayed decreased growth indicating that *NEK10* deletion compromised A549 cell transformation (Fig. 4*B*). Finally, upon tail vein injection into Nonobese diabetic/severe combined immunodeficiency (NOD/SCID) mice, *NEK10*$^{\Delta/\Delta}$ A549 lines exhibited reduced lung tissue colonization several weeks post injection, compared to controls, measured as cumulative tumor burden (Fig. 4*C*).

Discussion

Nek10 belongs to the family of Never in mitosis gene A (NIMA)-related cell cycle kinases, but unlike the other members which are serine-threonine kinases, it exhibits a preference for phosphorylation of tyrosines. We have previously reported a role for Nek10 in regulating a MAPK-activated G2/M checkpoint in response to UV irradiation (16). Since it is relatively highly expressed in the lung, we characterized the effect of Nek10 deletion in A549 cells, a line derived from an explant culture of a lung adenocarcinoma tumor, harboring a *KRAS* G12S oncogenic driver mutation. This led us to identify a function in modulating p53 following DNA damage (17). A nearly five-fold increase in the baseline protein levels of β-catenin in both the signaling and adherens junctions pools of the same cells led to the realization of a relationship between Nek10 and β-catenin described here (Fig. 1 and *SI Appendix*, Fig. S3*A*).

Mechanistically, Nek10 associates with the Axin complex and phosphorylates β-catenin at Tyr30, proximal to the well-characterized GSK3 phosphorylation sites at Ser33, Ser37, and Thr41 (*SI Appendix*, Fig. S8*A* and Fig. 2 *B*–*D*). Tyrosine phosphorylation of full-length β-catenin by Nek10 was significantly impaired by mutating Tyr30 suggesting that it is a bona fide and preferred Nek10 target site in vitro (Fig. 2*D*). The human β-catenin sequence contains seventeen Tyrosines, three of which, the aforementioned Tyr30 (YL motif), Tyr64 (YE motif), and Tyr333 (YE motif) are predicted to be phosphorylated by Nek10 (15). As the YE motif offers only marginal specificity for Nek10 phosphorylation, the residual phosphotyrosine signal in the Y30F mutant reactions is likely a product of Nek10 phosphoryation of β-catenin at Tyr64 and Tyr333. Previous work has implicated Tyr30 as one of three β-catenin tyrosines phosphorylated by Janus kinase 3 (Jak3), contingent upon prior phosphorylation of Tyr654, but the biological significance of Tyr30 was not further investigated in isolation (20). Of note, our in vitro kinase reactions were carried out in the absence of Axin, which might serve as a scaffold for this process within cells and affect the specificity and dynamics of phosphate transfer.

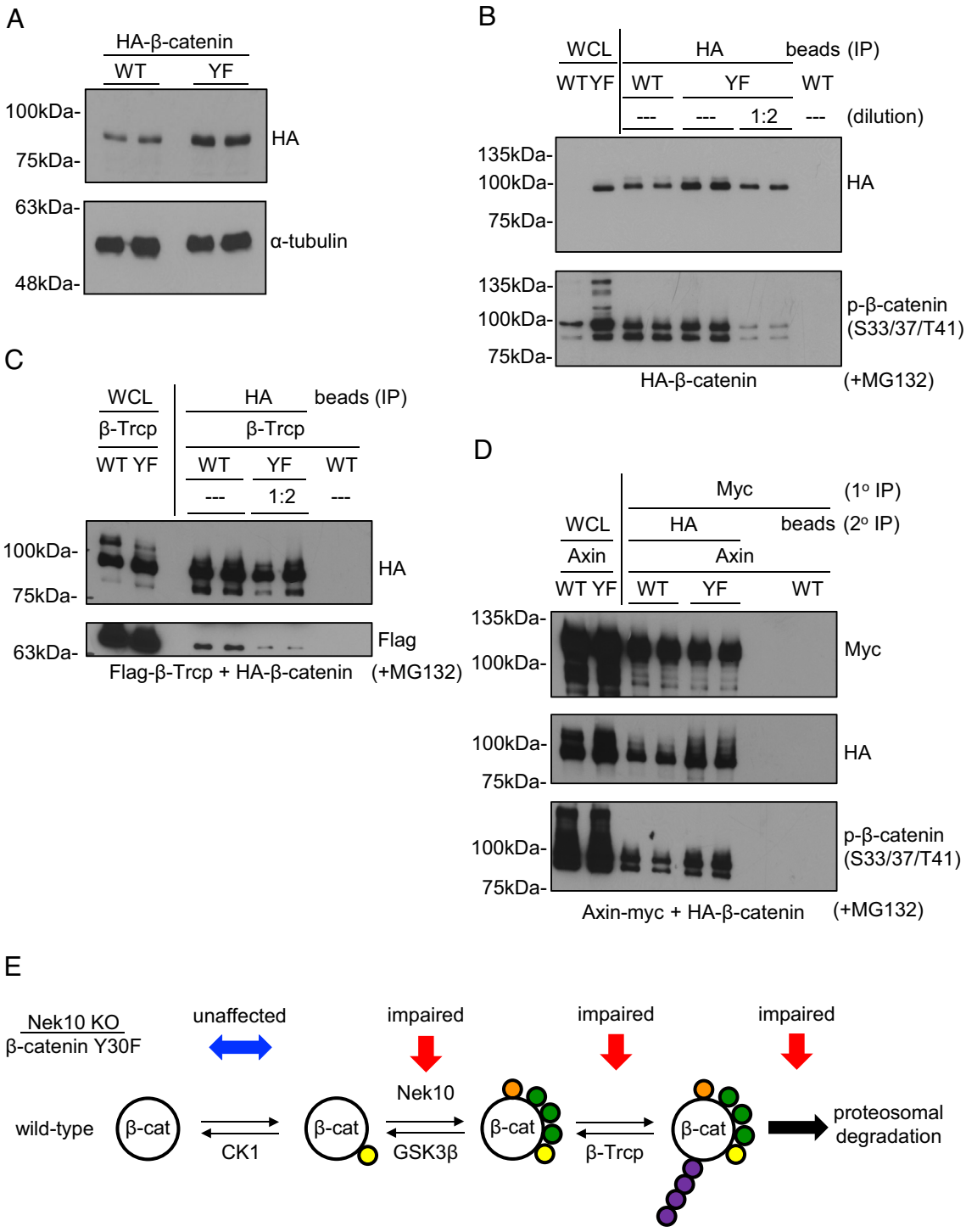

Fig. 3. Loss of Nek10 phosphorylation at tyrosine 30 impedes GSK3β mediated- phosphorylation of β-catenin and increases its cellular levels. (*A*) The levels of HA-tagged WT and mutant (Y30F) β-catenin exogeneously expressed in HEK293T cells. (*B*) The levels of Ser33/Ser37/Thr41 phosphorylation in immunoprecipitated HA-tagged WT and mutant (Y30F) β-catenin. Since the mutant protein is expressed at higher levels, phospho-antibody signals were normalized to the levels of total β-catenin in the immunoprecipitates. Cells were treated with MG132. (*C*) Comparison of Flag-tagged β-Trcp coimmunoprecipitating with HA-tagged WT and mutant (Y30F) β-catenin. The immunoprecipitated mutant β-catenin was diluted to facilitate comparison with the WT protein. Cells were treated with MG132. (*D*) The amount of total and Ser33/Ser37/Thr41 phosphorylated HA-tagged WT and mutant (Y30F) β-catenin coimmunoprecipitating with Myc-tagged Axin. To separate HA-tagged β-catenin from the endogeneous protein, Myc-Axin immunoprecipitates (primary IP) were first eluted and then reimmunoprecipitated with anti-HA (secondary IP). Cells were treated with MG132. (*E*) A graphical depiction of the proposed role of Nek10 in turnover of the β-catenin protein within the Axin complex. The effect of Nek10 deficiency, either through Crispr deletion or Y30F mutation, is also denoted.

CK1-phosphorylation of β-catenin at Ser45 primes the GSK3 phosphorylation events by effectively substituting a missing activation loop threonine phosphorylation that is characteristic of many kinases but not GSK3 (21). Nek10 phosphorylation, while not similarly required, does appear to promote GSK3 phosphorylation as evidenced by the reduction in the relative levels of GSK3-phosphorylated β-catenin in Nek10-deficient A549 cells. As there is more β-catenin available to enter the Axin complex in *NEK10*$^{\Delta/\Delta}$ cells, the levels of CK1-phosphorylated β-catenin are correspondingly elevated (Fig. 1*D*). By contrast,

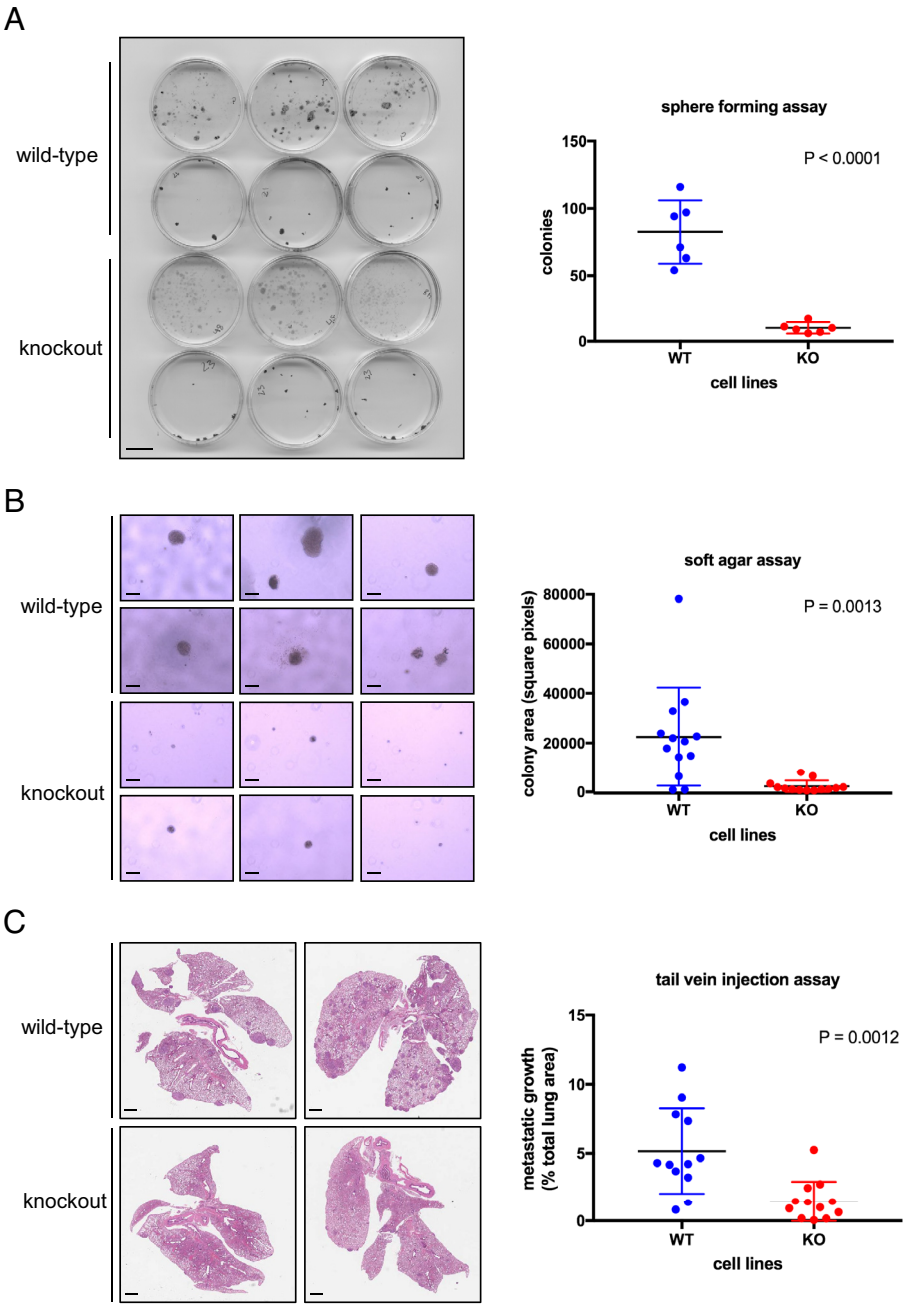

Fig. 4. Effect of Nek10 loss on A549 cell function. (*A*) The capacity of $NEK10^{+/+}$ and $NEK10^{\Delta/\Delta}$ A549 cells to form tumorspheres in suspension was evaluated (unpaired *t* test, n = 6, error bars represent SD). Scale represents 10 mm. (*B*) Anchorage-independent growth of $NEK10^{+/+}$ and $NEK10^{\Delta/\Delta}$ A549 lines was assessed in soft agar assays. Images of four random fields per cell line were analyzed for total collective area of colony growth (unpaired *t* test, n = 6, error bars represent SD). Scale represents 200 μm. (*C*) In vivo tumorigenicity was characterized by determining the ability of $NEK10^{+/+}$ and $NEK10^{\Delta/\Delta}$ cells to colonize NOD/SCID mouse lung tissue following tail vein injections. Metastatic growth was quantified by semiautomated digital analysis (unpaired *t* test, n = 8, error bars represent SD). Scale represents 1 mm.

GSK3-phosphorylated β-catenin is lower in the Nek10-deficient A549 lines despite greater substrate availability (Fig. 1*D*). Total cellular GSK3 kinase activity is unaffected by the loss of Nek10 implying that its effect is specific to GSK3 activity within the Axin complex (*SI Appendix*, Fig. S5).

While an association between Nek10 and Axin was observed upon their purification from HEK293T cells, no direct interaction between Nek10 and β-catenin could be detected (*SI Appendix*, Fig. S8 *A* and *B*). GSK3 has been reported to be constitutively associated with the Axin complex in HEK293T cells (19). Thus, it appears that Nek10 does not actively recruit β-catenin to the degradation complex, but is rather constrained to Tyr30 phosphorylation, to confer a kinetic advantage to the GSK3-mediated kinase reactions (Fig. 3*E*).

Blocking phosphorylation of Nek10's target site in β-catenin (Y30F) led to stabilization of the expressed mutant protein, phenocopying the effect of Nek10 deletion in A549 cells (Fig. 3*A* and *SI Appendix*, Fig. S6*C*). Moreover, relative GSK3-phosphorylation of the mutant β-catenin was also reduced, mimicking the observations in A549 cells (Fig. 3*B*). This in turn led to a relative reduction in the recruitment of the β-Trcp Ubiquitin E3 ligase, explaining the elevated levels of the mutant protein (Fig. 3*C*). A kinetic assessment of Wnt signaling throughput found that the efficiency of the Axin-mediated turnover correlated with the

relative amount of GSK3-phosphorylated β-catenin (22). Under conditions of Wnt stimulation, suboptimal degradation causes an accumulation of β-catenin until a new equilibrium is established, balancing the greater substrate availability with the impaired efficiency of β-catenin turnover, thereby preventing an indefinite rise in β-catenin levels. The absence of Nek10 phosphorylation appears to drive a similar, albeit constitutive, equilibrium. Indeed, compared with the WT protein, more Y30F mutant β-catenin was physically associated with Axin, consistent with the difference in the total cellular levels between the two (Fig. 3*D*). It should be noted that under conditions of Wnt signaling, GSK3-phosphorylated β-catenin has been found to accumulate in both Axin-bound and Axin-free cytosolic pools, revealing that at least a portion of phosphorylated β-catenin can dissociate from the Axin complex (7). This might explain why impairment in GSK3-mediated phosphorylation of the Y30F mutant would be more readily apparent at a cellular level than in the specifically Axin-associated pool of β-catenin.

Exogenously expressed WT and mutant β-catenin were appropriately localized to both the signaling and adherens junction pools, with Y30F mutant levels elevated in both (*SI Appendix*, Fig. S6 *A* and *B*). Moreover, both the WT and mutant protein responded as expected to Wnt-3a, LiCl, and MG132 treatments (*SI Appendix*, Fig. S7). Interestingly, the mutant β-catenin stabilized at higher levels in the presence of Wnt-3a, LiCl, and MG132, suggesting that the effect of Nek10 phosphorylation is independent of those treatments, thereby creating an additive effect.

In the course of this study, we also observed an increase in E-cadherin levels in Nek10$^{\Delta/\Delta}$ A549 cells. Since β-catenin stabilizes E-cadherin by protecting it from endocytosis and E-cadherin shelters β-catenin from the Axin complex, elevated β-catenin and E-cadherin frequently co-occur in lung tumors and more generally (23). It is therefore noteworthy that shRNA-mediated diminution of E-cadherin levels in Nek10-deficient A549 cells did not reverse the β-catenin stabilization phenotype, demonstrating that elevated β-catenin described here is linked to Nek10 and not E-cadherin status (*SI Appendix*, Fig. S4*B*).

Elevated β-catenin in Nek10-deficient A549 lines correlated with impaired proliferation of tumorspheres in suspension, anchorage-independent growth in soft agar, and the ability to colonize the lungs of NOD/SCID mice following tail vein injections (Fig. 4). Collectively, these results suggest that Nek10 loss might impair lung tumorigenesis and are consistent with the observed correlation between reduced Nek10 levels and improved clinical outcome in human lung cancer (*SI Appendix*, Fig. S2). Nevertheless, these findings stand in contrast to previous studies that found that increased β-catenin in the signaling pool generally promotes tumorigenesis and correlates with poor clinical prognosis, and might reflect a particular cellular context of which A549 cells are an exemplar. As noted, one feature of the Nek10-deficient A549 cell lines is the upregulation of β-catenin in both the adherens junctions and signaling pools. Oncogenic β-catenin upregulation in other cell models, for instance resulting from APC mutations, is observed primarily in the signaling pool. Further understanding of possible contextual distribution of elevated β-catenin between the distinct pools would benefit from expanding the present studies to a broader array of lung cancer lines, including those driven by other oncogenic drivers, such as mutant EGFR, to inform whether the observed phenotype represents a general consequence of Nek10 deficiency in lung cancer models. The fact that mutation of the Nek10 target site in β-catenin expressed in HEK293T cells phenocopies the effects of Nek10 deletion in A549 cells implies wider existence of such mechanism.

It has also been speculated elsewhere that the Wnt pathway operates within a "just right" paradigm, in which some measure of regulatory control is retained even within tumorigenic conditions to ensure optimal signaling output (24). This might be particularly pertinent to A549 cells which are already driven by the mutant *KRAS* oncogene, coupled with the partially diminished p53 response we previously observed upon Nek10 deletion (17). As sphere-forming assays are commonly interpreted as a measure of self-renewing cells within a bulk population, the altered tumorigenic potential of Nek10-deficient A549 cells could also reflect changes in stem cell capacity as suggested by impairment of Nek10-deficient cells in tumorsphere formation.

Detailed insight into Nek10 regulation via control of its expression in normal and malignant tissue, as well as posttranslational modifications resulting from upstream signaling throughput, will offer further perspective on its biology. A recent study identified a short mutational insertion in the Nek10 sequence, which destabilized the protein, in a small number of individuals presenting with idiopathic respiratory disease, suggesting that Nek10 abundance may have a broader impact on respiratory function (25). Beyond this, little is known about the factors which affect Nek10 levels via either transcriptional or protein regulation means.

In summary, our work establishes a previously unrecognized function for Nek10 in regulation of β-catenin affecting both its signaling and adherens junctions pools in A549 lung adenocarcinoma cells. Nek10 associates with the Axin complex in cells and phosphorylates β-catenin at Tyr30 located proximal to the regulatory sites responsible for controlling β-catenin turnover. In the absence of Nek10, the GSK3-mediated phosphorylation of β-catenin, a step known to be critical for modulating cellular β-catenin levels, was noticeably impaired. Nek10 deletion also correlated with reduced tumorigenic potential of A549 cells in several cellular and in vivo assays, consistent with current clinical data, possibly implicating Nek10 status as a prognostic marker and therapeutic target in lung and other cancers.

Materials and Methods

Antibodies. The following antibodies were used for western blotting, immunoprecipitations, and immunofluorescence: total β-catenin (1:2,000) (Cell Signaling #9562), phospho-β-catenin S33/S37/T41 (1:1,000) (Cell Signaling #9561), phospho-β-catenin S45 (1:1,000) (Cell Signaling #9564), α-tubulin (1:2,000) (Cell Signaling #2144), PARP (1:1,000) (Cell Signaling #9542), pY99 (1:500) (Santa Cruz sc-7020), HA (1:1,000) (Cell Signaling #3724), Myc (1:1,000) (Cell Signaling #2276), Flag (1:100,000) (Sigma #F3165), GST (1:1,000) (Cytiva 27-4577-01), E-cadherin (1:1,000) (BD #610181), E-cadherin (Proteintech #20874-1-AP), phospho-Lrp6 S1490 (1:1,000) (Cell Signaling #2568), phospho-Tau S202/T205 (1:1,000)(Cell Signaling #30505). Secondary antibodies used for western blotting were anti-rabbit-HRP (1:5,000 or 1:10,000) (Jackson ImmunoResearch #115-035-003), anti-mouse-HRP (1:5,000 or 1:10,000) (Jackson ImmunoResearch #111-035-003), IRDye 800CW goat anti-mouse (1:16,666) (LI-COR Biosciences #926-32210), IRDye 680RD goat anti-mouse (1:33,333) (LI-COR Biosciences #926-68070). Where applicable, western blotting dilutions are denoted in parentheses.

Constructs and Cloning. Generation of the Flag-Nek10 constructs has been described elsewhere (16). Axin1 was PCR amplified from HT29 cDNA and cloned as an EcoRI/XbaI fragment into pcDNA3.1-myc(C-terminal). β-catenin was amplified from MCF10A cDNA and cloned initially as a KpnI/ApaI fragment into pcDNA3.1-myc(C-terminal), then transferred into pcDNA3.1-HA(N-terminal) as a NotI/ApaI fragment and as a BamHI/NotI fragment into pGEX-4T3 for bacterial expression. The Y30F point mutation was introduced using the QuickChange site-directed mutagenesis kit (Stratagene). The Y30E point mutation was introduced using the Q5 site-directed mutagenesis kit (New England Biolabs). GST-ICAT was generated by amplifying a BamHI/XhoI fragment containing ICAT from BT474 cDNA and cloning

into pGEX-4T3. The ICAT cDNA was then cloned as a HindIII/EcoRI fragment into p3XFlag-CMV for mammalian expression. Flag-β-Trcp was amplified from A549 cDNA and cloned into p3XFlag-CMV as a NotI/BamHI fragment. Flag-Tau was amplified from T47D cDNA and cloned into p3XFlag-CMV as a NotI-BglII fragment.

Cell Culture. The generation of the Nek10-KO A549 cell lines has been described previously (17). E-cadherin was subsequently knocked down in two independent Nek10-KO A549 lines by transfecting an shRNA construct (Clone ID: TRCN0000039666) (Sigma) and isolating stable clonal cell lines in 2 μg/mL puromycin. A549, HEK293T, as well as control and Wnt-3a-producing L cells were maintained in DMEM supplemented with 10% fetal bovine serum. Control- and Wnt-3a-conditioned media were generated by passaging L cells at a 1:20 dilution and collecting the supernatant after 96 h which was then passed through a 0.45 μm filter. When required, unless otherwise specified, cells were treated with 10 μM MG132 for 4 h, 30 mM LiCl for 6 h, control- and Wnt-3a-conditioned media diluted with an equal volume of regular growth media for 6 h.

Cell Lysis and Immunoprecipitation. Cells were disrupted in lysis buffer containing 50 mM Tris (pH 7.5), 150 mM NaCl, 1 mM Ethylenediaminetetraacetic acid (EDTA), 1 mM Ethylene glycol-bis(β-aminoethyl ether)-N,N,N′,N′-tetraacetic acid (EGTA), 1% Triton, 1 mM Dithiothreitol (DTT), 1 mM sodium orthovanadate, 10 mM sodium glycerophosphate, 20 mM sodium fluoride, and protease inhibitor cocktail (Roche). Immunoprecipitations were generally carried out with 1 mg total lysate incubated with 1 μg of primary antibody overnight followed by 90 min with Protein A or Protein G sepharose beads and eluted with 2× Sodium dodecyl sulfate (SDS) sample loading buffer. In order to specifically assess exogeneous HA-tagged β-catenin association with Axin, without interference from the endogeneous protein, a two-step immunoprecipitation was carried out as follows. Myc-tagged Axin was immunoprecipitated from 5 mg lysate with 4 μg of anti-Myc antibody in a volume of 2.5 mL overnight, followed by 90 min with Protein G sepharose beads. Washed beads were eluted for 15 min with 100 μL 0.2 M glycine pH 2.6 supplemented with phosphatase and protease inhibitors. The eluates were first neutralized with 50 mM Tris pH 8.0, then diluted tenfold for the secondary immunoprecipitation with 1 μg anti-HA overnight followed by 90 min with Protein A sepharose beads. Immunoprecipitations undertaken to assess β-catenin phosphorylation or the association between β-catenin and β-Trcp were carried out on cells treated for 3 h with 10 μM MG132 to enable detection. Where required, western blots were analyzed either by Image J (26) or Odyssey application software (LI-COR).

Subcellular Fractionation. Cell pellets (3×10^6 cells) were washed with Phosphate buffered saline (PBS) and resuspended in 150 μL buffer A (10 mM 4-(2-hydroxyethyl)-1-piperazineethanesulfonic acid (HEPES) pH 7.9, 10 mM KCl, 1.5 mM $MgCl_2$, 0.34 M sucrose, 10% glycerol, 1 mM DTT, protease inhibitors). Minimal detergent (0.1% Triton) was gently added to the resuspended cells which were then subjected to a low-speed spin at 3,500 rpm for 5 min following a 7 min incubation on ice. The supernatant was clarified at 14,000 rpm for 5 min yielding the cytosolic fraction. The pellet from the low-speed spin was washed once in buffer A, resuspended in buffer B (3 mM EDTA, 0.2 mM EGTA, 1 mM DTT, protease inhibitors) for 15 min on ice, then spun at 4,000 rpm for 5 min with the supernatant retained as the nuclear fraction.

Recombinant Protein Expression and Purification. Competent BL21(DE3) *E. coli* were transformed with the relevant bacterial expression constructs. GST-ICAT was purified from cultures induced at $OD_{600} = 0.6$ with 0.5 mM Isopropyl ß-D-1-thiogalactopyranoside (IPTG) for 3 h at 37 °C. Bacterial pellets were disrupted by sonication (5 × 15 s) in 50 mM Tris (pH 7.5), 150 mM NaCl, 1 mM EDTA, 1 mM EGTA, 1% Triton, 5% glycerol supplemented with protease inhibitor cocktail (Roche). Recombinant GST-ICAT was batch purified by nutating clarified supernatant with glutathione beads for 2 h at 4 °C, followed by two washes with the above lysis buffer and an additional two washes with a reduced-detergent lysis buffer containing 0.1% Triton. Washed beads were eluted with 50 mM Tris (pH 8), 150 mM NaCl, 1 mM EDTA, 5% glycerol, and 30 mM glutathione for 1 h at 4 °C. Purified GST-ICAT was then dialyzed against 15 mM Tris (pH 7.5), 300 mM NaCl, and 5% glycerol for long-term storage. Purification of recombinant Nek10 and GST-β-catenin was carried out as described elsewhere (17).

ICAT Pulldown Assay. ICAT pulldown assays were performed by nutating 1 mg of cell lysate with 10 μg of purified GST-ICAT and glutathione sepharose beads in 1 mL total volume for 2 h at 4 °C, followed by three washes with lysis buffer and elution with 2× SDS sample loading buffer.

β-catenin Reporter (TOP-Flash) Assay. pGL3-BARL (Firefly luciferase) and pRL-TK (Renilla luciferase) constructs were a kind gift from Stephane Angers, University of Toronto. pGL3-BARL and pRL-TK were transfected into A549 cells at a 4:1 ratio by FuGENE HD (Promega) per the manufacturer's instructions. Luciferase activity was quantified by the Dual-Luciferase Assay System (Promega) per the manufacturer's instructions using a Hidex Sense plate reader.

Immunofluorescence. A549 cells were grown on coverslips, fixed with 4% paraformaldehyde for 15 min at room temperature, permeabilized with PBS/0.1% Triton for 10 min at room temperature, blocked with PBS/0.1% Triton/5% normal goat serum (NGS) for 1 h at room temperature, then incubated overnight at 4 °C with the β-catenin primary antibody (1:1,000) in PBS/0.1% Triton/5% NGS. The next day coverslips were washed three times with PBS/0.1% Triton and incubated with the anti-rabbit Alexa 488 secondary antibody for 1 h at room temperature. Coverslips were washed three times with PBS, counterstained with DAPI for nuclear visualization, mounted in Mowiol (Sigma), and then analyzed by confocal microscopy.

Kinase Assays. The ability of Nek10 to in vitro phosphorylate β-catenin was evaluated using both radioactive and nonradioactive assays. In the radioactive assay, purified recombinant Nek10 (WT or KD) was used to phosphorylate β-catenin immunoprecipitated from either $NEK10^{+/+}$ or $NEK10^{\Delta/\Delta}$ A549 cells. Reactions were carried out for 30 min at 30 °C in 40 μL volume containing 50 mM 3-(N-morpholino) propanesulfonic acid (MOPS) (pH7.4), 10 mM $MgCl_2$, 10 mM $MnCl_2$, 2 mM EGTA, 20 mM sodium glycerophosphate, 1 mM DTT, 5 μM Adenosine triphosphate (ATP), and 5 μCi [γ-^{32}P]ATP. Reactions were terminated with 2× SDS sample loading buffer, separated by SDS Polyacrylamide gel electrophoresis (SDS-PAGE), and detected by autoradiography. The nonradioactive assay was carried out similarly using recombinant Nek10 kinase, but with recombinant purified GST or GST-β-catenin (WT or Y30F mutant) as the substrate, and omitting [γ-^{32}P]ATP from the reactions, which were resolved by SDS-PAGE and detected by western blot with pY99 antibody. To facilitate comparison of the WT and Y30F mutant, the reactions were first terminated with 30 mM EDTA rather than sample loading buffer. The substrate was then purified by diluting the quenched reactions to 1 mL with pulldown assay buffer (final 50 mM Tris pH7.6, 150 mM NaCl, and 0.1% Triton), incubating with GST beads for 2 h, and eluting with 2× sample loading buffer. Eluates were resolved by SDS-PAGE and detected by western blot with pY99 antibody.

GSK3 Activity Assay. The levels of GSK3 activity in A549 cells were evaluated by monitoring the levels of exogeneous Tau phosphorylation at Ser202/Thr205. Since endogeneous Tau is expressed sparingly in A549 cells, $NEK10^{+/+}$ and $NEK10^{\Delta/\Delta}$ lines were transfected with a Flag-Tau construct. Exogeneous Tau was immunoprecipitated from cell lysates 48 h later and Tau phosphorylation in the immunoprecipitates determined using a phospho-Tau antibody.

Tumorsphere Assay. A549 cells were trypsinized, resuspended in sphere-forming media consisting of serum-free DMEM/F12 supplemented with B27 (1:50), 20 ng/mL EGF, 20 ng/mL FGF, and 10 μg/mL insulin, and then plated at 1,000 cells/well in a 6-well plate. After 2 wk of growth, cultures were spiked with 10% fetal bovine serum overnight to permit attachment for quantification.

Soft Agar Assay. Assays were carried out in 35 mm low attachment plates. A base layer was prepared consisting of 2 mL regular growth media supplemented with 0.7% low melt agarose. The top layer had 1,000 cells/plate in 1 mL regular growth media supplemented with 0.35% low melt agarose. Cells were grown for 2 wk with fresh growth media added every 4 d. Plates were imaged and colony growth quantified using ImageJ.

Tail Vein Injection Assay. A549 cells were trypsinized, resuspended in PBS, and 1×10^5 cells were injected in 100 μL into the tail veins of 12-wk-old NOD/SCID mice. The animals used in these experiments were housed in the UHN animal facilities accredited by the Canadian Council on Animal Care and treated in accordance with the institutional guidelines and the UHN Animal Care Committee-approved protocols. After 6 wk, mice were euthanized with CO_2, after which the lungs were dissected, fixed in 10% formalin, sectioned, and stained with hematoxylin and eosin (H&E) for analysis. Lung metastasis area was quantified by semiautomated digital analysis using QuPath pathology and bioimage analysis software (27). Briefly, digital images of H&E-stained lung sections were loaded into a single project file. The *Simple Tissue Detection* command was first used

to batch process the selection of lung tissue and exclusion of white space on all images, followed by manual annotation of each tissue sample and exclusion of staining artifacts. A random trees–based pixel classifier was manually trained to detect normal tissue and metastatic regions and then applied to each annotated lung section. Detections of metastasis made by the classifier were converted to annotation-type objects, and area measurements of each annotation were automatically tabulated. Percent tumor area was then calculated by first totaling the area of all tumor detections within a given lung annotation and dividing this sum by the area of the parent lung annotation.

Bioinformatics. Nek10 expression in human tissues was evaluated using the GTEx (Genotype–TissueExpression) portal. The GTEx Project was supported by the Common Fund of the Office of the Director of the NIH, and by NCI, NHGRI, NHLBI, NIDA, NIMH, and NINDS. Nek10 expression in mouse tissues was derived from RNAseq data deposited in the NCBI gene expression omnibus (28) from two independent studies, GSE41637 (29) and GSE74747 (30). The correlation between Nek10 expression levels and clinical outcome in patients with lung adenocarcinomas was evaluated using KM-plotter (31). The analysis was run, exclusively on adenocarcinomas, using a combined dataset which includes the following cohorts: TCGA, CAARRAY, GSE14814, GSE19188, GSE29013, GSE30219, GSE31210, GSE3141, GSE31908, GSE37745, GSE43580, GSE4573, GSE50081, and GSE8894.

Data, Materials, and Software Availability. All study data are included in the article and/or *SI Appendix*.

ACKNOWLEDGMENTS. This work was supported by the Canadian Institutes of Health Research Project Grant (174994). L.P. was a recipient of The Princess Margaret Hospital Foundation Graduate Fellowships in Cancer Research.

1. R. Jackstadt, M. C. Hodder, O. J. Sansom, WNT and β-catenin in cancer: Genes and therapy. *Annu. Rev. Cancer Biol.* **4**, 177–196 (2020).
2. A. M. Khalaf *et al.*, Role of Wnt/β-catenin signaling in hepatocellular carcinoma, pathogenesis, and clinical significance. *J. Hepatocell. Carcinoma* **5**, 61–73 (2018).
3. E. C. Pacheco-Pinedo *et al.*, Wnt/β-catenin signaling accelerates mouse lung tumorigenesis by imposing an embryonic distal progenitor phenotype on lung epithelium. *J. Clin. Investig.* **121**, 1935–1945 (2011).
4. S. Nakayama *et al.*, β-catenin contributes to lung tumor development induced by EGFR mutations. *Cancer Res.* **74**, 5891–5902 (2014).
5. K. W. Pond, K. Doubrovinski, C. A. Thorne, Wnt/β-Catenin signaling in tissue self-organization. *Genes* **11**, 939 (2020).
6. Z. Steinhart, S. Angers, Wnt signaling in development and tissue homeostasis. *Development* **145**, dev146589 (2018).
7. J. P. Gerlach, B. L. Emmink, H. Nojima, O. Kranenburg, M. M. Maurice, Wnt signalling induces accumulation of phosphorylated β-catenin in two distinct cytosolic complexes. *Open Biol.* **4**, 140120 (2014).
8. T. Valenta, G. Hausmann, K. Basler, The many faces and functions of β-catenin. *EMBO J.* **31**, 2714–2736 (2012).
9. E. M. Verheyen, C. J. Gottardi, Regulation of Wnt/β-catenin signaling by protein kinases. *Dev. Dyn.* **239**, 34–44 (2010).
10. E. C. van Kappel, M. M. Maurice, Molecular regulation and pharmacological targeting of the β-catenin destruction complex. *Br. J. Pharmacol.* **174**, 4575–4588 (2017).
11. R. Nusse, H. Clevers, Wnt/β-catenin signaling, disease, and emerging therapeutic modalities. *Cell* **169**, 985–999 (2017).
12. A. M. Fry, R. Bayliss, J. Roig, Mitotic regulation by NEK kinase networks. *Front. Cell Dev. Biol.* **5**, 102 (2017).
13. L. Moniz, P. Dutt, N. Haider, V. Stambolic, Nek family of kinases in cell cycle, checkpoint control and cancer. *Cell Div.* **6**, 1–10 (2011).
14. A. P. de Oliveira *et al.*, Checking NEKs: Overcoming a bottleneck in human diseases. *Molecules* **25**, 1778 (2020).
15. B. van de Kooij *et al.*, Comprehensive substrate specificity profiling of the human nek kinome reveals unexpected signaling outputs. *Elife* **8**, e44635 (2019).
16. L. S. Moniz, V. Stambolic, Nek10 mediates G 2 /M cell cycle arrest and MEK autoactivation in response to UV irradiation. *Mol. Cell. Biol.* **31**, 30–42 (2011).
17. N. Haider *et al.*, NEK10 tyrosine phosphorylates p53 and controls its transcriptional activity. *Oncogene* **39**, 5252–5266 (2020).
18. A. S. Flozak, A. P. Lam, C. J. Gottardi, A simple method to assess abundance of the β-catenin signaling pool in cells. *Methods Mol. Biol.* **1481**, 49–60 (2016).
19. V. S. W. Li *et al.*, Wnt signaling through inhibition of β-catenin degradation in an intact Axin1 complex. *Cell* **149**, 1245–1256 (2012).
20. X. Mishra, J. Das, N. Kumar, Janus kinase 3 regulates adherens junctions and epithelial mesenchymal transition through β-catenin. *J. Biol. Chem.* **40**, 16406–16419 (2017).
21. B. W. Doble, J. R. Woodgett, GSK-3: Tricks of the trade for a multitasking kinase. *J. Cell Sci.* **116**, 1175–1186 (2003).
22. A. R. Hernández, A. M. Klein, M. W. Kirschner, Kinetic responses of β-catenin specify the sites of Wnt control. *Science* **338**, 1337–1340 (2012).
23. R. Sormunen, P. Pääkkö, R. Kaarteenaho-Wiik, Y. Soini, Differential expression of adhesion molecules in lung tumours. *Histopathology* **50**, 282–284 (2007).
24. C. Albuquerque *et al.*, The 'just-right' signaling model: APC somatic mutations are selected based on a specific level of activation of the β-catenin signaling cascade. *Hum. Mol. Genet.* **11**, 1549–1560 (2002).
25. R. R. Chivukula *et al.*, A human ciliopathy reveals essential functions for NEK10 in airway mucociliary clearance. *Nat. Med.* **26**, 244–251 (2020).
26. C. A. Schneider, W. S. Rasband, K. W. Eliceiri, NIH Image to ImageJ: 25 years of image analysis. *Nat. Methods* **9**, 671–675 (2012).
27. P. Bankhead *et al.*, QuPath: Open source software for digital pathology image analysis. *Sci. Rep.* **7**, 16878 (2017).
28. T. Barrett *et al.*, NCBI GEO: Archive for functional genomics data sets–Update. *Nucleic Acids Res.* **41**, D991–D995 (2013).
29. J. Merkin, C. Russell, P. Chen, C. B. Burge, Evolutionary dynamics of gene and isoform regulation in Mammalian tissues. *Science* **338**, 1593–1599 (2012).
30. M. A. Huntley *et al.*, Complex regulation of ADAR-mediated RNA-editing across tissues. *BMC Genomics* **17**, 61 (2016).
31. A. Lánczky, B. Győrffy, Web-based survival analysis tool tailored for medical research (KMplot): Development and implementation. *J. Med. Internet Res.* **23**, e27633 (2021).